Optimising ozone control strategies for Chinese megacity clusters under the influence of stratospheric intrusion

Kaihui Zhao[1], Wen Chen[1,*], Puyu Lian[2] and Danni Xu[1]

[1]Yunnan Key Laboratory of Meteorological Disasters and Climate Resources in the Greater Mekong Subregion, Yunnan University, Kunming, 650091, China

[2]School of Environment and Energy, South China University of Technology, Guangzhou, 510006, China

Corresponding author: Wen Chen (chenwen-dq@ynu.edu.cn)

Abstract

Stratosphere intrusion (SI), the largest natural source of ozone (O_3), poses a significant challenge for policymakers in developing effective O_3 control strategies. Understanding the emission reduction pathway under SI influence is crucial for achieving long-term O_3 attainment. However, the role of SI in tropospheric O_3 pollution in China remains poorly understood. To develop effective O_3 control strategies, we employed a localised comprehensive air quality model and the Whole Atmosphere Community Climate Model (WACCM). We found that SI contributions vary seasonally, peaking in spring and reaching a minimum in summer. Spatially, SI impacts surface O_3 most in high-latitude regions, decreasing with lower latitudes. As O_3-laden air reaches the surface, O_3 control strategies become less effective, necessitating additional emission reductions. As SI contributions increase, the optimal emission reduction pathway shifts: for the BTH and PRD regions, it changes from 'VOC only' to 'NO_x only' at thresholds of 13.57 ppb and 8.39 ppb, respectively. For YRD, FWP, and CY, the 'VOC only' path remains optimal. This study provides valuable insights for policymakers to develop effective strategies to mitigate SI's negative effects.

Keywords*:* stratospheric intrusion; ozone pollution; ozone precursor sensitivity; emission reduction pathways

Plain Language Summary

Stratospheric intrusion (SI) presents a significant challenge to policymakers attempting to formulate effective O_3 control strategies, as it introduces natural variability that can undermine anthropogenic emission reduction efforts. By analyzing temporal and spatial variations of SI and its effects on surface O_3, our study identifies optimal emission reduction pathways tailored to five megacity clusters. Our findings highlight the necessity of adapting emission reduction approaches based on SI contributions, which vary seasonally and geographically. This nuanced approach is crucial for achieving long-term O_3 attainment and improving air quality in megacity clusters, which are often hotspots of pollution and human activity.

1 Introduction

Tropospheric ozone (O_3) is gaining increased public attention because of its impacts on human health, ecosystem productivity, and climate change. Numerous studies have highlighted changes in O_3 precursor emissions and regional transport, as well as the contribution from the stratosphere, all influencing observed trends and variability in tropospheric O_3 (Brown-Steiner & Hess, 2011; Hess & Zbinden, 2013; Li et al., 2024; Lin et al., 2012). Therefore, understanding the role of stratospheric intrusion (SI) in determining tropospheric and surface-layer O_3 variations is crucial for effectively mitigating ground-level O_3 pollution.

SI represents a significant natural source of tropospheric O_3 (Zhao et al., 2021; Das et al., 2016; Xia et al., 2023), which can cause surface O_3 concentrations to exceed the national ambient air quality standard (NAAQS). Verstraeten et al. (2015) indicated that contributions from SI can partly offset the effects of policy-driven emission control strategies in the western US. Meanwhile, a modelling study demonstrated that maximum hourly O_3 concentrations reached 88 ppbv during a deep SI event (Langford et al., 2012). Lin et al. (2012) observed that SI contributed 15–20 ppbv at high-elevation surface sites in the western US. Then, in later work, by extending the study period to 23 years, Lin et al. (2015) found that approximately 15–25 ppbv of surface O_3 in the spring was transported from the stratosphere. Zhang et al. (2016) used a global chemical transport model to quantify the contribution of SI to surface O_3 in northern China, finding values of around 3–20 $\mu g \cdot m^{-3}$ in summertime. The US Environmental Protection Agency (EPA) classifies SI as a natural event that can be considered exceptional under the Clean Air Act and exceptional events rule criteria, allowing policymakers to exclude such data for non-attainment identification (https://www.epa.gov/air-quality-analysis/treatment-air-quality-monitoring-data-influenced-exceptional-events). As the largest natural source of tropospheric O_3, a poor understanding of the contribution of SI will hinder the formulation of the exemption criteria used for exceptional SI events in China.

As a secondary pollutant, O_3 responds nonlinearly to its precursors – namely, volatile organic compounds (VOCs) and nitrogen oxides (NO_x – the sum of NO (nitric oxide) and NO_2 (nitrogen dioxide)) – under different levels of O_3 precursor sensitivity (OPS) (Ou et al., 2016; Turnock et al., 2018; Zhao et al., 2022). Studies in China have shown that O_3 reduction varies significantly along different emission reduction pathways (Ou et al., 2016; Ding et al., 2022; Liu et al., 2013). For example, in an NO_x-limited regime, NO_x control reduces O_3 levels, whereas NO_x reduction increases O_3 concentrations in a VOC-limited regime. Ou et al. (2016) found that VOC-focused controls are effective for short-term O_3 reduction, while NO_x-focused controls are more efficient for significant O_3 reductions. As external downward transport from the stratosphere further aggravates surface O_3 pollution, it is necessary to strengthen emission reduction efforts to counteract the negative impact of SI (Zhao et al., 2022; Ni et al., 2019; Stohl et al., 2003). Considering the response of O_3 to different emission reduction pathways, the extent of reduction and prioritisation of specific species may need to be dynamically adjusted (Luecken et al., 2018; Zhu et al., 2024). Thus, it is imperative to understand the optimal emission reduction pathways for megacity clusters in China under the influence of SI to mitigate O_3 pollution effectively.

SI plays a crucial role in surface O_3 pollution, diminishing the effectiveness of emission reduction strategies. Therefore, it is vital to establish appropriate emission reduction pathways considering the influence of SI, especially in the most developed city clusters. However, the role of SI in tropospheric O_3 pollution in China remains poorly understood. To address this knowledge gap and develop effective O_3 control strategies, we employed a localized comprehensive air quality model and the Whole Atmosphere Community Climate Model (WACCM) to explore the following questions: (1) What are the spatial and temporal characteristics of SI over five megacity clusters in China? (2) What are the spatial and temporal variations in the contributions of SI? (3) What is the optimal emission reduction pathway for different megacity clusters under the influence of SI? This study has significant implications for establishing criteria for determining exceptional SI events and identifying optimal emission reduction pathways for megacity clusters in China amidst climate change.

2 Materials and Methods

2.1 WACCM

WACCM is an interdisciplinary collaboration integrated into CESM (the Community Earth System Model). It encompasses upper-atmospheric, middle-atmospheric, and tropospheric modelling from three laboratories of the US National Center for Atmospheric Research (NCAR): HAO (High Altitude Laboratory), ACOM (Atmospheric Chemistry Observations & Modeling), and CGD (Climate & Global Dynamics), respectively.

Meteorological fields are supplied by NASA's GMAO GEOS-5 model. Anthropogenic emissions are based on the latest inventory from CAMS (the Copernicus Atmospheric Monitoring Service). Open fire emissions are calculated using FINN-v1 (Fire Inventory from NCAR, version 1.0) (Wiedinmyer et al., 2011). The model outputs are available for analysis at 6-h intervals, with a horizontal resolution of 0.9° latitude × 1.25° longitude and 88 vertical levels spanning from 1000 to 1 hPa.

The model includes complex stratospheric chemistry, a representation of the QBO (Quasi-Biennial Oscillation), and non-orographic gravity waves, which have been successfully used in stratospheric O_3 simulations and to simulate stratosphere–troposphere exchange processes (Butchart et al., 2010; Oberlaender et al., 2013).

We utilized AIRS data, O_3 sounding data, and ERA5 data to validate WACCM results. The concentration and position of the O_3 enhancement area from the model agreed well with the AIRS retrieved data, O_3 sounding data and ERA5 data. The aforementioned data collectively indicate that during the spring season in Hong Kong, there is a tongue-shape plume of high O_3 concentrations extending from the stratosphere, resulting in the formation of a O_3 enhancement within the lower troposphere **(Figure S1)**. These results give us confidence that WACCM results can well capture the SI process.

To track SI contributions, we used stratospheric O_3 and biomass burning CO (carbon monoxide) tagging approaches. These methods help to quantify the amount of tropospheric O_3 originating from the stratosphere and the impact of biomass burning (Akritidis et al., 2016; Wiedinmyer et al., 2011; Matthes et al., 2010). The O_3S tracer was set to stratospheric values above the tropopause, and the chemical loss rate was observed in the troposphere.

2.2 WRF-Chem simulation

The Weather Research and Forecasting model coupled with Chemistry (WRF-Chem), version 3.9.1, was used for numerical simulations of meteorological conditions and air quality during the spring seasons of 2020–2022. The outer domain (D1) covers all of China with a horizontal resolution of 27 km; the middle domain (D2) encompasses most of central and eastern

China with a 9-km resolution; and the innermost domains cover five megacity clusters – BTH, YRD, PRD, FWP, and CY – at a grid resolution of 3 km. Vertically, 46 layers were set from the lowest vertical layer of 40 m to the 50-hPa level. Outputs from Whole Atmosphere Community Climate Model (WACCM) are used to provide chemical initial and lateral conditions to the WRF-Chem simulations. The land use data used in the simulations are retrieved from the Moderate Resolution Imaging Spectroradiometer (MODIS) observation. **Figure S2** shows that WRF-Chem model has good performance for O_3, with averaged correlation coefficient (R) of 0.63 over China. The averaged normalized mean error (NME) is 29%.

To identify local emission reductions to offset the impact of SI, 1 base case and 39 emission reduction scenarios with anthropogenic VOCs (AVOCs) and NO_x emission reductions were used to identify the OPS. Since biogenic VOC (BVOC) emissions are difficult to control, emission reduction scenarios were applied only to AVOCs. Therefore, in sensitivity studies for emission reduction experiments, the model concentrates on numerous compounds of VOCs, including isoprene, benzene, toluene, propylene, ethylene, xylenes, propane, acetylene, butanes, pentanes, and organic acids.

2.3 AIRS satellite

The Atmospheric Infrared Sounder (AIRS) onboard NASA’s Aqua satellite provides detailed vertical profiles of O_3 concentrations with a horizontal resolution of 1° × 1° and 24 vertical levels ranging from 1000 to 1 hPa. Data from AIRS offer valuable insights into the distribution of O_3, aiding in monitoring O_3 layer changes, atmospheric chemistry, and climate dynamics. These data can be accessed at https://airs.jpl.nasa.gov/data/get-data/standard-data/.

3 Results

3.1 General characteristics of SI-related O_3 enhancement in the lower troposphere

Since Beijing-Tianjin-Hebei (BTH), Yangtze River Delta (YRD), Pearl River Delta (PRD) are the three most developed city clusters with high population and severe air pollution, and the 14th Five-Year Plan listed Fenwei Plain (FWP), and Chengyu (CY) as new key areas which deserve a detailed investigation. Moreover, in the 2024 ‘Blue Sky Defence War Project’, the five regions have been identified as key areas for air pollution prevention and control in China. As seen in **Figure S3**, the changing emissions of O_3 precursors and the inflow of stratospheric O_3 are considered primary sources of elevated tropospheric O_3 concentrations over China, from upward and downward directions, respectively. Anthropogenic emissions of NOx and VOCs hotspots are notably concentrated in these five megacity clusters. The high intensity of VOCs and NOx emissions serves as a fundamental cause for the frequent occurrence of O_3 pollution events.

To analyse the spatiotemporal distribution of O_3 over these five megacity clusters, a time–height cross-sectional plot of monthly averaged O_3 profile observations from the past 21 years (2003–2023) is shown in **Figure 1**. A prominent tongue-shaped plume with high O_3 concentrations extending from the stratosphere is apparent in all five clusters. During winter and spring, a notable buildup of O_3 in the UTLS (upper troposphere and lower stratosphere) region significantly impacts lower-tropospheric and even surface O_3 levels. The SIs first occur in subtropical regions such as the PRD (22°N–25°N), YRD (29°N–32°N), and CY (28°N-32°N) during spring, and then gradually move northward to FWP (33°N–39°N) and BTH (36°N–42°N) in summer. The seasonal movement and intensity of the subtropical jet account for the time lag in SI occurrence (Zhao et al., 2021).

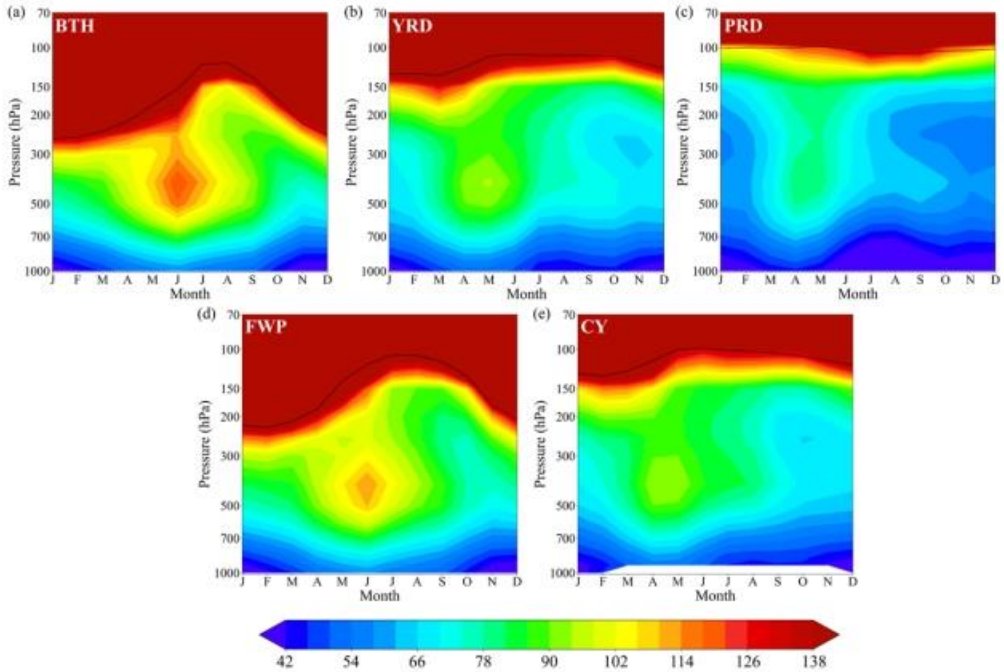

Figure 1. Seasonal variations of monthly averaged O_3 (unit: ppb) retrieved by AIRS from 2003 to 2023 in (a) BTH, (b) YRD, (c) PRD, (d) FWP, and (e) CY. The black solid line denotes the tropopause height.

O_3 enhancement (approximately 80–90 ppbv) can be seen above 500 hPa in April and May in YRD, PRD, and CY. Comparatively, the O_3 pool, exceeding 110 ppbv, appears progressively later at higher latitudes, peaking in BTH and FWP in June. Seasonal O_3 variation is mainly due to favourable meteorological conditions in summer, such as strong solar radiation and high temperatures. Such a significant O_3 hotspot with concentrations above 80 ppbv in the lower troposphere can exacerbate surface O_3 pollution alongside strong descending motion. However, the East Asian summer monsoon impacts O_3 levels, reducing them to below 40 ppbv between 700 and 850 hPa in PRD.

To fully understand the impact of SI over the five megacity clusters, a more comprehensive assessment is needed. However, the annual variation in SI occurrence has not been thoroughly investigated. We identified SI events using the following criteria, which have been proposed and widely applied in previous studies for screening stratospheric intrusion events (Zhao et al., 2021; Beekmann et al., 1997; Brioude et al., 2007; Kim & Lee, 2010): (a) relative humidity of less than 25%; (b) wind speed higher than 20 m/s; and (c) O_3 levels of 25% above the climatological mean. Considering the latitude-dependent decline in tropopause height, we selected SI events based on the Potential Vorticity (PV) exceeding 0.5 PVU (1 PVU = 1.0×10^{-6} m^2 s^{-1} K kg^{-1}) in PRD, and 2 PVU in YRD, CY, FWP, and BTH. Due to the pronounced characteristic of lower tropopause heights in the northern regions and higher heights in the southern regions, there are significant differences in the defined potential vorticity (PV) thresholds for determining tropopause height. Thus, two PV values were used in this study. In addition, it should be noted that the mean PV, relative humidity, wind, and O_3 within the 200-300 hPa range are calculated as the criteria. These data used to identify SI events are analyzed using hourly data from the fifth-generation European Centre for Medium-Range Weather Forecasts atmospheric reanalysis (ERA5).

As shown in **Table 1**, with these criteria, the total numbers of SI events from 2000 to 2023 were 1383, 1250, 342, 941, and 867 for BTH, YRD, PRD, FWP, and CY, respectively, averaging 57.6, 52.1, 14.3, 39.2, and 36.1 events per year. The highest SI frequency in middle latitudes is largely related to the descending branch of the local tropical Northern Hemisphere Hadley cell (Roelofs & Lelieveld, 1997; Meul et al., 2018). A high tropopause fold frequency in YRD and CY enhances the potential for SI occurrence, with average frequencies of 10.2 and 11.7, respectively (**Figure S4**). Previous studies also suggest that stratospheric overturning circulation can be strengthened by El Niño and the easterly shear Quasi-Biennial Oscillation and hence increase the downward transport of stratospheric O_3-enriced air to the mid-latitude upper troposphere (Neu et al., 2014; Bronnimann et al., 2004; Randel et al., 2009). For BTH and FWP, SI is facilitated by cut-off low and upper level trough systems in mid-to-high-latitude regions, as corroborated by previous studies (Li et al., 2015; Li & Bian, 2015; Chen et al., 2024). The frequency of SI events fluctuated greatly from 2000 to 2023: 44–80 times in BTH, 33–67 times in YRD, 2–33 times in PRD, and 29–50 times in both FWP and CY. These fluctuations are primarily influenced by factors such as high-level jet movements (Zhao et al., 2021), extratropical cyclones (Jiang et al., 2015), El Niño–Southern Oscillation (ENSO) (Lin et al., 2015; Albers et al., 2022), tropopause folding (Wimmers & Moody, 2004), and Rossby wave-breaking (Waugh et al., 1994). Although many studies suggest that SI impacts will increase in response to a strengthened Brewer–Dobson circulation (BDC) under climate change (Meul et al., 2018; Butchart et al., 2010; Oberländer et al., 2013), our results do not indicate such a trend in these five megacity clusters over the past two decades. The impact of climate change on SI varies by latitude, climate scenario, and ENSO event type, necessitating further investigation.

Over the past decade, O_3 concentrations have exhibited high-level oscillations, contrasting with decreases in other pollutants, as shown in **Figure 2**. From 2015 to 2019, the annual O_3 concentration in the five megacity clusters increased yearly by 6.3 $\mu g/(m^3 \cdot yr)$. From 2019 to 2021, annual O_3 concentrations decreased to 2017–2018 levels but rebounded significantly in 2022.

BTH, YRD, FWP, and CY experienced the most photochemical O_3 exceedances (i.e., not influenced by exceptional events) from May to September, peaking in June and July. In PRD, O_3 pollution mainly occurred from September to November, influenced by favourable weather conditions such as clear skies, high temperatures, and typhoons. From late May to August, O_3 exceedances due to SIs or typical conditions were able to occur. Rare O_3 exceedances in March and April, highlighted in red, are more likely influenced by SI and differ from usual early-spring conditions (**Figure 2**). BTH and YRD had the highest SI-related O_3 exceedances with 47 and 43 days, respectively, followed by FWP with 30 days and PRD with 25 days. Due to the relatively low number of NAAQS exceedance days in CY and the mismatch with SI occurrence, CY had only three SI-related O_3 exceedance days. As seen in **Figure S5**, the majority of SIs occur on days characterized by low O_3 pollution levels. This phenomenon is particularly notable during the winter and spring months, which coincide with the active seasons for SI. Compared to the other three regions, BTH and YRD have over 100 days of SI events falling within days when O_3 concentrations exceed 100 $\mu g/m^3$, indicating that under the context of climate change, as O_3

pollution intensifies further and SI becomes more active, the number of O_3 exceedance days in BTH and YRD may further increase in the future.

Table 1. Total number of SI cases over BTH, YRD, PRD, FWP, and CY from 2000 to 2023.

	BTH	YRD	PRD	FWP	CY
2000	64	45	7	44	46
2001	50	47	6	34	39
2002	44	37	2	36	32
2003	51	52	10	30	26
2004	55	56	23	34	36
2005	51	43	16	30	23
2006	45	47	6	38	44
2007	60	57	9	48	45
2008	69	60	18	47	50
2009	66	60	31	39	43
2010	63	47	5	29	28
2011	80	46	17	46	27
2012	66	53	6	45	37
2013	61	63	19	50	38
2014	50	60	10	45	37
2015	61	55	16	45	34
2016	53	53	22	42	43
2017	49	56	15	43	25
2018	59	46	16	31	31
2019	47	49	21	32	41
2020	61	55	15	36	40
2021	57	67	8	35	35
2022	61	63	33	43	42
2023	60	33	11	39	25
Sum	1383	1250	342	941	867
Mean	57.6	52.1	14.3	39.2	36.1

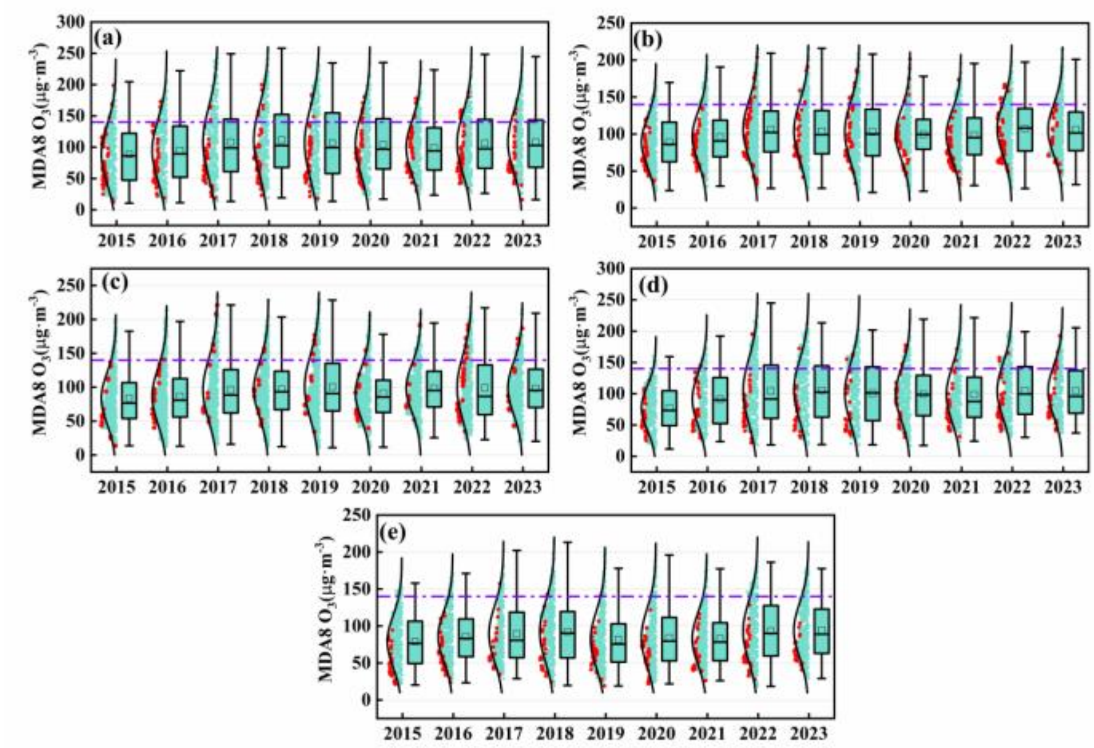

Figure 2. Boxplot analysis of maximum daily 8-hour average (MDA8) O_3 concentrations from 2015 to 2023 in (a) BTH, (b) YRD, (c) PRD, (d) FWP, and (e) CY. The red circles denote SI-influenced days, and the purple dashed line represents the NAAQS of 140 μg/m^3.

3.2 Quantification of the impact of SIs on tropospheric O_3

As discussed, SI is a critical factor driving temporal and spatial variations in tropospheric O_3. The contribution of SI varies greatly depending on its intensity, with deep SI events able to transport O_3-rich air into the lower troposphere, thereby significantly enhancing lower-tropospheric O_3 during springtime, particularly in middle and high latitudes (Zhao et al., 2021; Monks, 2000); while in contrast, shallow SI events have a weaker impact on lower-tropospheric O_3 (Stohl et al., 2003). To quantify the contributions of SI to tropospheric O_3 in the five megacity clusters investigated in this study, we used the stratospheric O_3 tagging approach, as detailed in the Methods section.

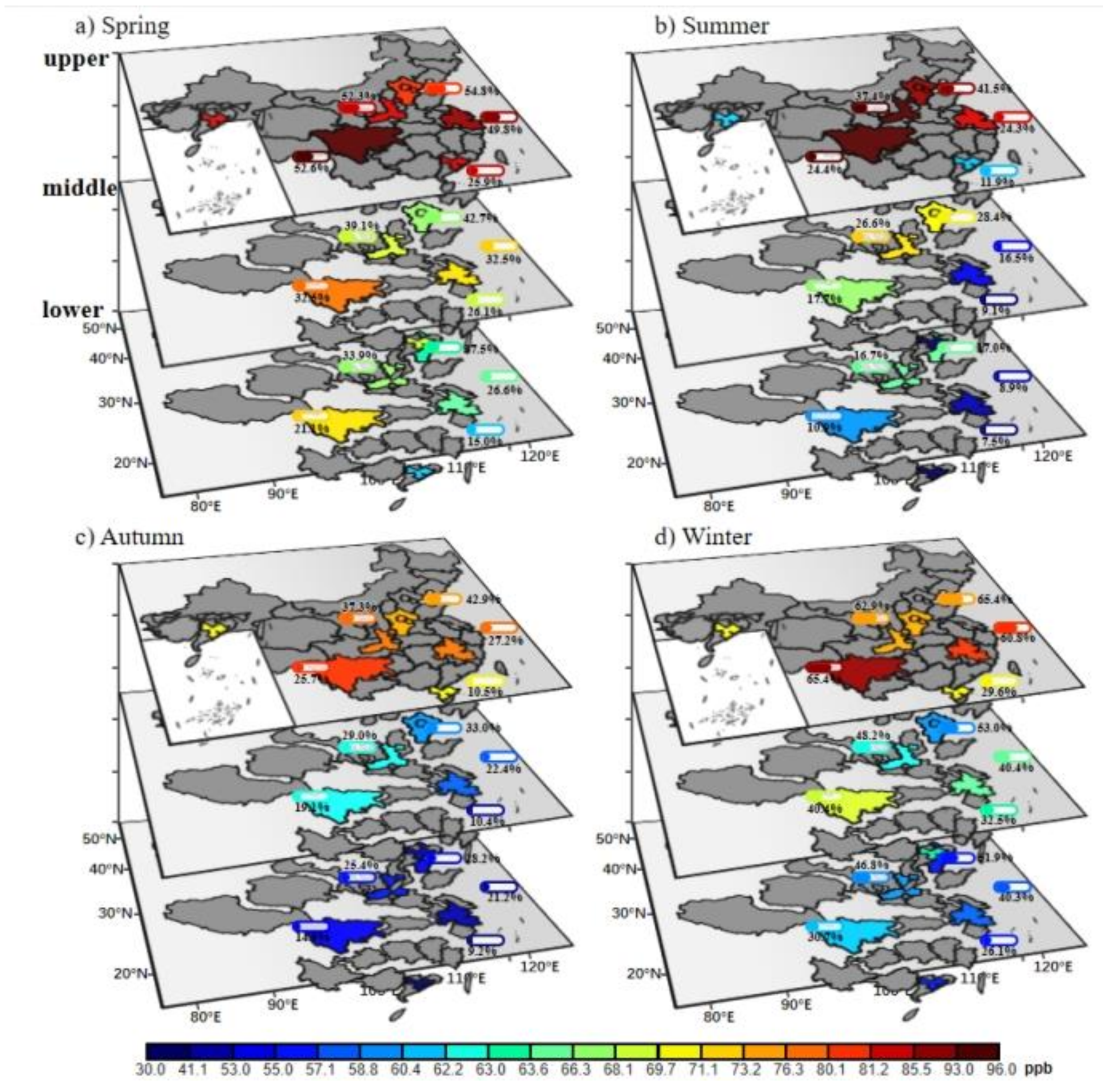

Figure 3. Seasonal variations of the contribution of SI to O_3 (unit: ppbv) at different levels in (a) spring, (b) summer, (c) autumn, and (d) winter. The percentage contributions of SI to tropospheric O_3 are highlighted by the bars.

Figure 3 shows a positive correlation between O_3 and O_3S in all five megacity clusters, indicating the significant impact of SI on tropospheric O_3. Injected stratospheric O_3 contributed largely to tropospheric O_3 enhancement during SI periods, reaching up to 60% in the upper troposphere, suggesting a dominant role of SI in upper-tropospheric O_3 variations in recent years. Temporally, contributions from SI exhibited strong seasonality, with the largest impact in spring, followed by winter and summer, and the smallest in autumn. The reason for this seasonal characteristic is mainly related to the strengthening upper troposphere baroclinic activities, higher tropopause folding frequency, and upper tropospheric jet stream movements in spring and winter. Vertically, contributions from SI decreased with altitude, with the average O_3S/O_3 ratio being 40.1% in the upper troposphere and 24.5% in the lower troposphere. Spatially, the impacts of SI were most pronounced in mid-latitude regions, especially in spring, where contributions could reach

50%, 30%, and 20% in the upper, middle, and lower troposphere, respectively. The downward transport of stratospheric O_3 within the Hadley cell and frequent tropopause folds in mid-latitude regions likely caused the higher O_3S/O_3 ratio in the lower troposphere. In high-latitude regions, SI explained approximately 50%, 40%, 40%, and 60% of the upper-tropospheric O_3 during spring, summer, autumn, and winter, respectively. Due to lower tropopause heights in these regions, SI contributed an average of 16.7%–33.9% to lower-tropospheric O_3 enhancement during the O_3 season (spring, summer, and autumn). Comparatively, SI had less impact on tropospheric O_3 in lower-latitude regions, with contributions accounting for 7.5%–15% of lower-tropospheric O_3.

3.3 Quantification of the impact of SIs on surface O_3

In the previous section, we found that SI significantly impacts tropospheric O_3, with contributions varying across seasons and regions. However, the extent of the contribution of SI to surface O_3 in the five megacity clusters studied here remains unclear.

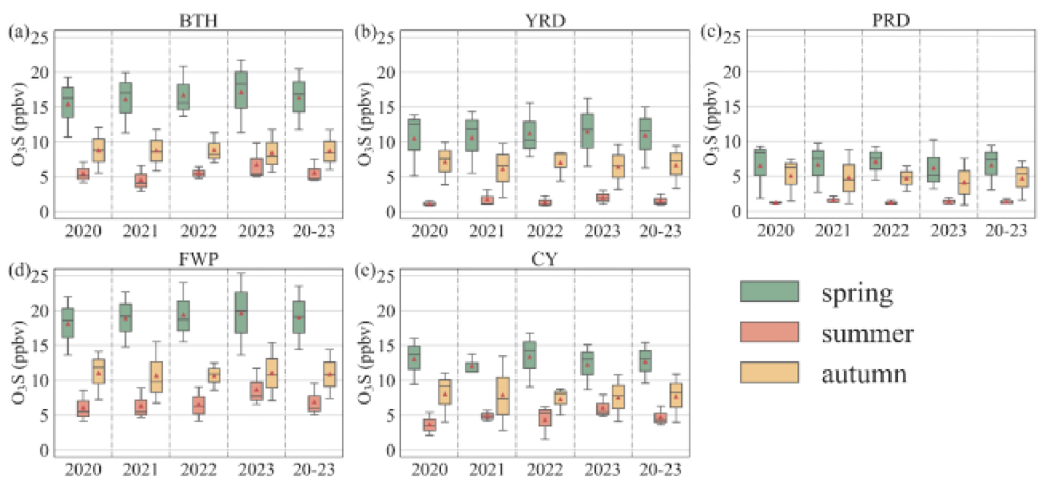

Figure 4. Annual variations of the contribution of SI to O_3 (unit: ppb) in the surface layer from 2020 to 2023 in (a) BTH, (b) YRD, (c) PRD, (d) FWP, and (e) CY. The bars in green, yellow, and purple represent spring, summer, and autumn, respectively.

Figure 4 reveals that the contributions of SI to surface O_3 followed an increasing trend over BTH, YRD, and FWP during spring from 2020 to 2023, with annual increases of 0.45, 0.25, and 0.39 ppb/yr, respectively. This increase would mainly have been due to the strengthened BDC and increased frequency of tropopause folds (Butchart et al., 2010; Oberländer et al., 2013; Akritidis et al., 2016). Notably, the maximum contribution of SI in spring occurred in March, with faster increasing rates of 0.61 ppb/yr in BTH, 0.60 ppb/yr in YRD, and 0.96 ppb/yr in FWP, suggesting that against the backdrop of climate change, contributions from SI may potentially be heightening the risk of springtime O_3 pollution, leading to an earlier onset of O_3 pollution.

Temporally, contributions from SI exhibited distinct seasonal patterns, with spring maxima and summer minima, closely related to high-level jet movements, tropopause folding, and tropospheric convective activities. Spatially, SI had the largest impact on surface O_3 in BTH and FWP, with seasonal average contributions of 16.36 and 19.02 ppb, respectively. SI contributed an average of 10.97 and 12.69 ppb to surface O_3 during 2020–2023 in YRD and CY, respectively. Compared to the other regions, SI had a limited impact on surface O_3 in PRD, with a contribution of only 6.62 ppb. This spatial heterogeneity can be attributed to the decreasing tropopause height with increasing latitude and the high frequency of tropopause folding. Our results highlight the significant impact of SI on the surface O_3 budget and its sensitivity to climate change, underscoring the necessity for developing clear criteria for identifying SI, especially on O_3 exceedance days.

3.4 Insights into refining O_3 control strategies

As discussed previously, SI can transport O_3-laden air from the stratosphere to the surface, necessitating additional controls on anthropogenic emissions to offset the negative impact of SI. Without accounting for contributions from SI, the effectiveness of O_3 control strategies may be significantly compromised.

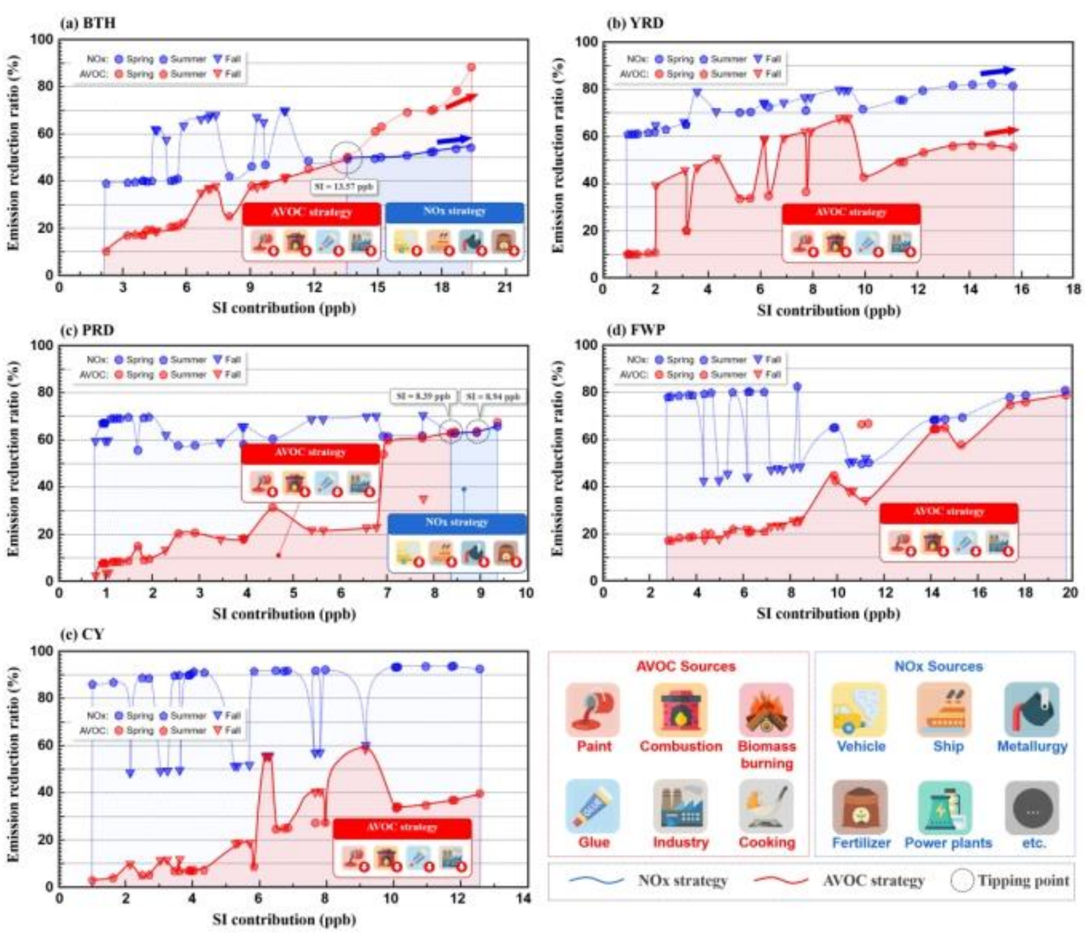

Figure 5. Extra emission reductions (unit: %) in response to the contributions of SI in (a) BTH, (b) YRD, (c) PRD, (d) FWP, and (e) CY. The red shading highlights priority control strategies focusing on AVOC emissions, while the blue shading highlights those focusing on NO_x emissions.

To date, the Chinese government has not considered the contributions from SI when formulating emission reduction strategies. Consequently, O_3 reductions may not achieve the desired outcomes. By conducting the sensitivity study introduced in Section materials and methods, we identified the optimal emission reduction pathways to offset SI contributions in BTH, YRD, PRD, FWP, and CY (**Figure 5)**.

Due to the negative impact of SI, greater emission reduction efforts are required to counteract the additional O_3 influx from the stratosphere in all five megacity clusters. As contributions from SI increase, more aggressive emission reduction strategies must be implemented. The greatest emission reductions to mitigate the impacts from SI across the five regions are needed in spring. Consequently, it is imperative to develop O_3 control strategies that carefully consider the impact of springtime SIs.

Additionally, due to the nonlinear relationship between O_3 and its precursors in different regions, there is significant spatial heterogeneity in the efficiency of emissions reduction to offset the impacts of SI. As contributions from SI increase, the optimal control pathways for the BTH and PRD regions shift from 'VOC only' to 'NO_x only', with thresholds of 13.57 and 8.39 ppb, respectively. However, the underlying mechanisms for this transition differ between the two regions. In BTH, significant SI contributions render the 'VOC only' pathway, although effective for short-term O_3 reduction, less efficient for long-term emissions reduction. Once the contributions from SI surpass certain thresholds, the 'NO_x only' pathway demonstrates a superior emissions reduction efficiency. In PRD, as NO_x emissions have gradually decreased in response to progressive atmospheric pollution control measures, O_3 formation has become increasingly sensitive to NO_x. The OPS is shifting from a VOC-limited regime to a transitional regime because of ongoing efforts in O_3 pollution control. For the other three regions, the 'VOC only' pathway remains the optimal emissions reduction strategy to offset contributions from SI. Additionally, the 'NO_x only' pathway incurs greater costs, and as contributions from SI increase, the gap in effectiveness between the two pathways gradually narrows.

Overall, to offset the extra contributions of SI, it is necessary to reduce O_3 concentrations through the mitigation of NO_x and VOCs. However, due to regional disparities in OPS, the required reductions for offsetting SI vary by region. Moreover, when the contribution of SI exceeds a certain threshold, the optimal reduction pathway may also undergo significant changes.

Against the backdrop of climate change, the global annual stratospheric intrusion O_3 flux increased by 53% from 2000 to 2100 under the Representative Concentration Pathway 8.5 Scenario (Meul et al., 2018). With intensifying SI activities and worsening springtime O_3 pollution, it is crucial to characterize SI behaviours to inform future O_3 control strategies. There are considerable disparities in VOCs and NO_x emissions across industries. Anthropogenic sources of VOCs emission primarily include fossil fuel combustion, biomass burning, oil and gas evaporation and leakage, solvent evaporation, petrochemical processes, cooking, and tobacco smoke. NO_x predominantly originates from industrial activities, transportation, and power plants. Therefore, for the BTH and PRD regions, when SI contributions exceed the local control capacity, policymakers need to dynamically adjust priorities to reduce O_3 precursors in specific industries, thereby offsetting the additional contribution from SI.

4 Conclusions

This study fills a critical gap in understanding the role of SI in tropospheric O_3 pollution in China and identifies optimal emission reduction pathways to counter the impacts of SI. Our findings highlight the need for additional emission reduction efforts to mitigate the adverse effects of SI. It is important to note, however, that our analysis focused on the impact of SI on seasonal mean O_3 levels, which is likely to be more severe during episodes of high O_3 pollution. Moreover, the OPS varies significantly across different regions and days, indicating that the most effective emission reduction strategies must be dynamically adjusted.

Although SIs are natural events beyond human control, they significantly affect air quality assessments. Unlike other exceptional events such as dust storms, identifying and attributing the contributions of SI to O_3 exceedances requires rigorous scientific evaluation and operational guidelines. To accurately reflect the outcomes of O_3 control strategies, adopting the US EPA's exceptional event guidance could improve the scientific validity and accuracy of air quality assessments in China.

SI events, driven mainly by atmospheric circulation dynamics and thermodynamics, significantly differ from anthropogenic emission sources near the surface. Therefore, it is crucial to exclude exceedance data from monitoring points during such events from air quality reports. In 2018, the US EPA released guidelines on 'Exceptional Events Demonstrations for Stratospheric Ozone Intrusions'. However, due to the lack of definitive evidence regarding SI occurrences and impacts in China, this study aimed to provide scientific assessments and operational guidelines.

China faces a critical period in its efforts to control O_3 pollution, necessitating stringent and detailed O_3 strategies. It is essential to assess the impact of SI on these strategies. Stratospheric O_3 intrusion contributes significantly to long-term surface background O_3 concentrations, potentially influencing China's long-term O_3 control policies. Thus, further scientific evaluation and research are needed to understand the extent of this impact.

In many previous studies, stratospheric O_3 tracing methods used in air quality models have been widely employed to track SI and quantify their contributions to tropospheric and near-surface O_3 (Lin et al., 2015; Emmons et al., 2003; Smith et al., 2014; Zhang et al., 2022). However, it should be noted that the simulation of O_3S by air quality model remains inherent uncertainties due to a fundamental flaw, which marks O_3 transported from the troposphere into the stratosphere as being of stratospheric origin. This approach leads to an overestimation of the contribution of stratospheric O_3 (Emmons et al., 2012; Hess & Lamarque, 2007). Hence, it is essential to further enhance the accuracy of SI quantification in the future by improving stratospheric O_3 chemical mechanisms, increasing the vertical resolution near the tropopause, and optimizing atmospheric physical and chemical processes within the model.

Moreover, under climate change, stronger downward airmass movements can facilitate the transport of accumulated stratospheric O_3 to the surface, thereby weakening the overestimation of simulated O_3S. Therefore, in the case that direct observations of stratospheric O_3 are not feasible due to technological limitations, simulation of O_3S is still an effective method to quantify the impact of SI with the rising trend of compound extreme synoptic events. If the impacts of SI are not considered, air quality and climate change mitigation policies may be less effective. Therefore, we conclude that addressing regional O_3 pollution and climate change requires considering the effects of SI.

The synergistic effect of air pollution reduction and carbon emissions has been significantly enhanced by carbon peaking and neutralisation efforts. Anthropogenic emissions have started to decrease noticeably, and the potential for further reducing VOC emissions is diminishing. Consequently, the pace of emissions reduction has slowed. To address the increased contribution of SI under climate change, it is crucial to quickly transition the OPS into an NO_x-limited regime. This strategy aims to mitigate the adverse impacts of SIs by focusing on reducing NO_x emissions.

Acknowledgments

This study is supported by the National Natural Science Foundation of China (No. 42465008), the National Natural Science Foundation of China (No. 42105164), the National Natural Science Foundation of China (No. 42405195), the Open Research Fund Program of Plateau Atmosphere and Environment Key Laboratory of Sichuan Province, grant number (No. PAEKL-2024-K01), Yunnan Science and Technology Department Youth Project (No. 202401AU070202), Guangdong Basic and Applied Basic Research Foundation (No. 2022A1515011078), Xianyang key research and development program (No. L2022ZDYFSF040).

Data availability

The stratospheric O_3 tracer was retrieved from the NCAR (https://www2.acom.ucar.edu/gcm/waccm). The meteorological data are available from fifth generation ECMWF atmospheric reanalysis of the global climate (https://www.ecmwf.int/en/forecasts/dataset/ecmwf-reanalysis-v5). The surface weather charts were provided by the Hong Kong Observatory (http://envf.ust.hk/dataview/hko_wc/current/). The WRF/Chem model code was downloaded from http://www2.mmm.ucar.edu/wrf. The anthropogenic emission data were obtained from http://www.meicmodel.org/.

References

Akritidis, D., Pozzer, A., Zanis, P., Tyrlis, E., Skerlak, B., Sprenger, M., & Lelieveld, J. (2016). On the role of tropopause folds in summertime tropospheric ozone over the eastern Mediterranean and the Middle East. *Atmospheric Chemistry and Physics*, *16*(21), 14025-14039. https://doi.org/10.5194/acp-16-14025-2016.

Albers, J. R., Butler, A. H., Langford, A. O., Elsbury, D., & Breeden, M. L. (2022). Dynamics of ENSO-driven stratosphere-to-troposphere transport of ozone over North America. *Atmospheric Chemistry and Physics*, *22*(19), 13035-13048. https://doi.org/10.5194/acp-22-13035-2022.

Beekmann, M., Ancellet, G., Blonsky, S., DeMuer, D., Ebel, A., Elbern, H. et al. (1997). Regional and global tropopause fold occurrence and related ozone flux across the tropopause. *Journal of Atmospheric Chemistry*, *28*(1-3), 29-44. https://doi.org/DOI 10.1023/A:1005897314623.

Brioude, J., Cammas, J. P., Zbinden, R. M., & Thouret, V. (2007). Evidence of tropospheric layering: interleaved stratospheric and planetary boundary layer intrusions. *Atmos. Chem. Phys. Discuss.*, *2007*, 1119-1142. https://doi.org/10.5194/acpd-7-1119-2007.

Brown-Steiner, B., & Hess, P. (2011). Asian influence on surface ozone in the United States: A comparison of chemistry, seasonality, and transport mechanisms. *Journal of Geophysical Research-Atmospheres*, *116*. https://doi.org/10.1029/2011JD015846.

Bronnimann, S., Luterbacher, J., Staehelin, J., Svendby, T. M., Hansen, G., & Svenoe, T. (2004). Extreme climate of the global troposphere and stratosphere in 1940-42 related to El Nino. *Nature*, *431*(7011), 971-974. https://doi.org/10.1038/nature02982.

Butchart, N., Cionni, I., Eyring, V., Shepherd, T. G., Waugh, D. W., Akiyoshi, H. et al. (2010). Chemistry-Climate Model Simulations of Twenty-First Century Stratospheric Climate and Circulation Changes. *Journal of Climate*, *23*(20), 5349-5374. https://doi.org/10.1175/2010JCLI3404.1.

Chen, Z., Liu, J., Qie, X., Cheng, X., Yang, M., Shu, L., & Zang, Z. (2024). Stratospheric influence on surface ozone pollution in China. *Nature Communications*, *15*(1). https://doi.org/10.1038/s41467-024-48406-x.

Das, S. S., Ratnam, M. V., Uma, K. N., Subrahmanyam, K. V., Girach, I. A., Patra, A. K. et al. (2016). Influence of tropical cyclones on tropospheric ozone: possible implications. *Atmospheric Chemistry and Physics*, *16*(8), 4837-4847. https://doi.org/10.5194/acp-16-4837-2016.

Ding, D., Xing, J., Wang, S., Dong, Z., Zhang, F., Liu, S., & Hao, J. (2022). Optimization of a NO x and VOC Cooperative Control Strategy Based on Clean Air Benefits. *Environmental Science & Technology*, *56*(2), 739-749. https://doi.org/10.1021/acs.est.1c04201.

Emmons, L. K., Hess, P., Klonecki, A., Tie, X., Horowitz, L., Lamarque, J. F. et al. (2003). Budget of tropospheric ozone during TOPSE from two chemical transport models. *Journal of Geophysical Research-Atmospheres*, *108*(D8). https://doi.org/10.1029/2002JD002665.

Emmons, L. K., Hess, P. G., Lamarque, J. F., & Pfister, G. G. (2012). Tagged ozone mechanism for MOZART-4, CAM-chem and other chemical transport models. *Geoscientific Model Development*, *5*(6), 1531-1542. https://doi.org/10.5194/gmd-5-1531-2012.

Hess, P. G., & Lamarque, J. (2007). Ozone source attribution and its modulation by the Arctic oscillation during the spring months. *Journal of Geophysical Research-Atmospheres*, *112*(D11). https://doi.org/10.1029/2006JD007557.

Hess, P. G., & Zbinden, R. (2013). Stratospheric impact on tropospheric ozone variability and trends: 1990 - 2009. *Atmospheric Chemistry and Physics*, *13*(2), 649-674. https://doi.org/10.5194/acp-13-649-2013.

Jiang, Y. C., Zhao, T. L., Liu, J., Xu, X. D., Tan, C. H., Cheng, X. H. et al. (2015). Why does surface ozone peak before a typhoon landing in southeast China? *Atmospheric Chemistry and Physics*, *15*(23), 13331-13338. https://doi.org/10.5194/acp-15-13331-2015.

Kim, J. H., & Lee, H. (2010). What causes the springtime tropospheric ozone maximum over Northeast Asia? *Advances in Atmospheric Sciences*, *27*(3), 543-551. https://doi.org/10.1007/s00376-009-9098-z.

Langford, A. O., Brioude, J., Cooper, O. R., Senff, C. J., Alvarez, R. J., Hardesty, R. M. et al. (2012). Stratospheric influence on surface ozone in the Los Angeles area during late spring and early summer of 2010. *Journal of Geophysical Research-Atmospheres*, *117*. https://doi.org/10.1029/2011JD016766.

Li, D., & Bian, J. C. (2015). Observation of a Summer Tropopause Fold by Ozonesonde at Changchun, China: Comparison with Reanalysis and Model Simulation. *Advances in Atmospheric Sciences*, *32*(10), 1354-1364. https://doi.org/10.1007/s00376-015-5022-x.

Li, D., Bian, J. C., & Fan, Q. J. (2015). A deep stratospheric intrusion associated with an intense cut-off low event over East Asia. *Science China-Earth Sciences*, *58*(1), 116-128. https://doi.org/10.1007/s11430-014-4977-2.

Li, Y., Xia, Y., Xie, F., & Yan, Y. (2024). Influence of stratosphere-troposphere exchange on long-term trends of surface ozone in CMIP6. *Atmospheric Research*, *297*. https://doi.org/10.1016/j.atmosres.2023.107086.

Lin, M., Fiore, A. M., Horowitz, L. W., Cooper, O. R., Naik, V., Holloway, J. et al. (2012). Transport of Asian ozone pollution into surface air over the western United States in spring. *Journal of Geophysical Research-Atmospheres*, *117*. https://doi.org/10.1029/2011JD016961.

Lin, M., Fiore, A. M., Horowitz, L. W., Langford, A. O., Oltmans, S. J., Tarasick, D., & Rieder, H. E. (2015). Climate variability modulates western US ozone air quality in spring via deep stratospheric intrusions. *Nature Communications*, *6*. https://doi.org/10.1038/ncomms8105.

Liu, H., Wang, X. M., Pang, J. M., & He, K. B. (2013). Feasibility and difficulties of China 's new air quality standard compliance: PRD case of PM2.5 and ozone from 2010 to 2025. *Atmospheric Chemistry and Physics*, *13*(23), 12013-12027. https://doi.org/10.5194/acp-13-12013-2013.

Luecken, D. J., Napelenok, S. L., Strum, M., Scheffe, R., & Phillips, S. (2018). Sensitivity of Ambient Atmospheric Formaldehyde and Ozone to Precursor Species and Source Types Across the United States. *Environmental Science & Technology*, *52*(8), 4668-4675. https://doi.org/10.1021/acs.est.7b05509.

Matthes, K., Marsh, D. R., Garcia, R. R., Kinnison, D. E., Sassi, F., & Walters, S. (2010). Role of the QBO in modulating the influence of the 11 year solar cycle on the atmosphere using constant forcings. *Journal of Geophysical Research-Atmospheres*, *115*. https://doi.org/10.1029/2009JD013020.

Meul, S., Langematz, U., Kroeger, P., Oberlander-Hayn, S., & Joeckel, P. (2018). Future changes in the stratosphere-to-troposphere ozone mass flux and the contribution from climate change and ozone recovery. *Atmospheric Chemistry and Physics*, *18*(10), 7721-7738. https://doi.org/10.5194/acp-18-7721-2018.

Monks, P. S. (2000). A review of the observations and origins of the spring ozone maximum. *Atmospheric Environment*, *34*(21), 3545-3561. https://doi.org/DOI 10.1016/S1352-2310(00)00129-1.

Neu, J. L., Flury, T., Manney, G. L., Santee, M. L., Livesey, N. J., & Worden, J. (2014). Tropospheric ozone variations governed by changes in stratospheric circulation. *Nature Geoscience*, *7*(5), 340-344. https://doi.org/10.1038/ngeo2138.

Ni, Z., Luo, K., Gao, X., Gao, Y., Fan, J., Fu, J. S., & Chen, C. (2019). Exploring the stratospheric source of ozone pollution over China during the 2016 Group of Twenty summit. *Atmospheric Pollution Research*, *10*(4), 1267-1275. https://doi.org/10.1016/j.apr.2019.02.010.

Oberländer, S., Langematz, U. & Meul, S. (2013). Unraveling impact factors for future changes in the Brewer-Dobson circulation. *Journal of Geophysical Research-Atmospheres*, *118*(18), 10296-10312. https://doi.org/10.1002/jgrd.50775.

Ou, J., Yuan, Z., Zheng, J., Huang, Z., Shao, M., & Li, Z. et al. (2016). Ambient Ozone Control in a Photochemically Active Region: Short-Term Despiking or Long-Term Attainment? *Environmental Science & Technology*, *50*(11), 5720-5728. https://doi.org/10.1021/acs.est.6b00345.

Randel, W. J., Garcia, R. R., Calvo, N., & Marsh, D. (2009). ENSO influence on zonal mean temperature and ozone in the tropical lower stratosphere. *Geophysical Research Letters*, *36*. https://doi.org/10.1029/2009GL039343.

Roelofs, G.-J. & Lelieveld, J. (1997). Model study of the influence of cross-tropopause O3 transports on tropospheric O3 levels. *Tellus Series B-Chemical and Physical Meteorology*, *49*(1), 38-55. https://doi.org/https://doi.org/10.1034/j.1600-0889.49.issue1.3.x.

Smith, K. L., Neely, R. R., Marsh, D. R., & Polvani, L. M. (2014). The Specified Chemistry Whole Atmosphere Community Climate Model (SC-WACCM). *Journal of Advances in Modeling Earth Systems*, *6*(3), 883-901. https://doi.org/10.1002/2014MS000346.

Stohl, A., Bonasoni, P., Cristofanelli, P., Collins, W., Feichter, J., Frank, A. et al. (2003). Stratosphere-troposphere exchange: A review, and what we have learned from STACCATO -: art. no. 8516. *Journal of Geophysical Research-Atmospheres*, *108*(D12). https://doi.org/10.1029/2002JD002490.

Turnock, S. T., Wild, O., Dentener, F. J., Davila, Y., Emmons, L. K., Flemming, J. et al. (2018). The impact of future emission policies on tropospheric ozone using a parameterised approach. *Atmospheric Chemistry and Physics*, *18*(12), 8953-8978. https://doi.org/10.5194/acp-18-8953-2018.

Verstraeten, W. W., Neu, J. L., Williams, J. E., Bowman, K. W., Worden, J. R., & Boersma, K. F. (2015). Rapid increases in tropospheric ozone production and export from China. *Nature Geoscience*, *8*(9), 690. https://doi.org/10.1038/NGEO2493.

Waugh, D. W., Plumb, R. A., Atkinson, R. J., Schoeberl, M. R., Lait, L. R., Newman, P. A. et al. (1994). Transport out of the lower stratospheric Arctic vortex by Rossby wave breaking. *Journal of Geophysical Research: Atmospheres*, *99*(D1), 1071-1088. https://doi.org/https://doi.org/10.1029/93JD02556.

Wiedinmyer, C., Akagi, S. K., Yokelson, R. J., Emmons, L. K., Al-Saadi, J. A., Orlando, J. J., & Soja, A. J. (2011). The Fire INventory from NCAR (FINN): a high resolution global model to estimate the emissions from open burning. *Geoscientific Model Development*, *4*(3), 625-641. https://doi.org/10.5194/gmd-4-625-2011.

Wimmers, A. J., & Moody, J. L. (2004). Tropopause folding at satellite-observed spatial gradients: 1. Verification of an empirical relationship. *Journal of Geophysical Research-Atmospheres*, *109*(D19). https://doi.org/10.1029/2003JD004145.

Xia, Y., Xie, F., & Lu, X. (2023). Enhancement of Arctic surface ozone during the 2020 - 2021 winter associated with the sudden stratospheric warming. *Environmental Research Letters*, *18*(2). https://doi.org/10.1088/1748-9326/acaee0.

Zhang, Y., Cooper, O. R., Gaudel, A., Thompson, A. M., Nedelec, P., Ogino, S., & West, J. J. (2016). Tropospheric ozone change from 1980 to 2010 dominated by equatorward redistribution of emissions. *Nature Geoscience*, *9*(12), 875. https://doi.org/10.1038/NGEO2827.

Zhang, Y., Li, J., Yang, W., Du, H., Tang, X., Ye, Q. et al. (2022). Influences of stratospheric intrusions to high summer surface ozone over a heavily industrialized region in northern China. *Environmental Research Letters*, *17*(9). https://doi.org/10.1088/1748-9326/ac8b24.

Zhao, K., Huang, J., Wu, Y., Yuan, Z., Wang, Y., Li, Y. et al. (2021). Impact of Stratospheric Intrusions on Ozone Enhancement in the Lower Troposphere and Implication to Air Quality in Hong Kong and Other South China Regions. *Journal of Geophysical Research-Atmospheres*, *126*(18). https://doi.org/10.1029/2020JD033955.

Zhao, K., Hu, C., Yuan, Z., Xu, D., Zhang, S., Luo, H. et al. (2021). A modeling study of the impact of stratospheric intrusion on ozone enhancement in the lower troposphere over the Hong Kong regions, China. *Atmospheric Research*, *247*. https://doi.org/10.1016/j.atmosres.2020.105158.

Zhao, K., Wu, Y., Yuan, Z., Huang, J., Liu, X., Ma, W. et al. (2022). Understanding the underlying mechanisms governing the linkage between atmospheric oxidative capacity and ozone precursor sensitivity in the Yangtze River Delta, China: A multi-tool ensemble analysis. *Environment International*, *160*. https://doi.org/10.1016/j.envint.2021.107060.

Zhu, Q., Schwantes, R. H., Coggon, M., Harkins, C., Schnell, J., He, J. et al. (2024). A better representation of volatile organic compound chemistry in WRF-Chem and its impact on ozone over Los Angeles. *Atmospheric Chemistry and Physics*, *24*(9), 5265-5286. https://doi.org/10.5194/acp-24-5265-2024.